JOURNAL OF THERMOPHYSICS AND HEAT TRANSFER
Vol. 15, No. 1, January–March 2001

Investigation of the Temperature Distribution on Radiator Fins with Micro Heat Pipes

Y. X. Wang*
Texas A&M University, College Station, Texas 77843-3123
H. B. Ma†
University of Missouri, Columbia, Missouri 65211
and
G. P. Peterson‡
Rensselaer Polytechnic Institute, Troy, New York 12180

A flexible micro-heat-pipe panel, fabricated by sintering an array of aluminum wires between two thin aluminum sheets, was developed as part of a program to develop lightweight, flexible radiator fin structures for use on long-term spacecraft missions. A numerical model, which combined both conduction and radiation effects, was established to predict the heat-transfer performance and temperature distribution of the radiator fin in a simulated space environment. Three different concepts are presented, evaluated, and discussed. Comparison of the predicted and experimental results indicated that the model developed herein can be used to accurately predict the temperature distribution and heat-transfer performance occurring in micro-heat-pipe radiators. This comparison further indicates that the flexible radiator with the array of micro heat pipes has an effective thermal conductivity of more than 20 times that of the uncharged version and 10 times that of a solid material. This results in a more uniform temperature distribution, which could significantly improve the overall radiation effectiveness, reduce the overall size, and meet or exceed the baseline design requirements for long-term manned missions to Mars.

Nomenclature

$A_{c,s}$ = superficial cross-section area, m^2
a = constant
c = constant
F = view factor
G = irradiation, W/m^2
J = radiosity, W/m^2
K_{eff} = effective thermal conductance, W/K
k = kth control volume
k_{eff} = effective thermal conductivity, W/K · m
L_{eff} = effective length, m
m = mass flow rate, kg/s
N = total number of surfaces
n = divided element number of radiator surface
q = heat flux, W/m^2
T = temperature, K
t = total thickness of micro-heat-pipe array, m
x = coordinate, m
y = coordinate, m
Δx = width of control volume in x direction, m
Δy = width of control volume in y direction, m
δ_{kj} = Kronecker delta
ε = emissivity
ρ = density, kg/m^3
σ = radiation constant, 5.67×10^{-8} W/(m^2 · K^4)

Subscripts

c = cold surface, condenser
ch = characteristic
e = environment, evaporator
k = kth finite element
r = radiator fin
x = x direction of coordinate system
y = y direction of coordinate system

Introduction

IN November 1997 NASA Johnson Space Center began a joint research and development effort with Lockheed Martin Vought Systems to design and develop a flexible, lightweight spacecraft radiator for Mars missions. The results of this joint effort concluded that a radiator built around a loop heat-pipe concept would be a very good candidate for long-term manned missions to Mars. In this design thermal energy generated inside the spacecraft would be transferred to solid radiator fins by a series of loop heat pipes. Once at the radiator fin, the heat would be conducted throughout the fin structure and then rejected to the space environment through radiation. Clearly, there are several very important parameters that govern the fin effectiveness, fin efficiency, and the radiator area to weight ratio. Among these are the conductivity of the fin structure and the radiator emissivity/absorptivity ratio.

Micro heat pipes have been successfully used in a number of applications for removal of heat, and because of their high effective thermal conductivity a high degree of temperature uniformity can be achieved across electronic devices.[1,2] In addition, micro heat pipes can be fabricated in virtually any shape, and through the use of thin flexible materials or thin metal laminates, it may be possible to meet the flexibility requirements for long-term Mars missions and to significantly reduce the total system weight.

Micro heat pipes are typically fabricated as a wickless, noncircular channel with a diameter of approximately the same dimensions as the characteristic radius of the liquid meniscus.[3] Since 1984, a number of investigations have been conducted in an effort to better understand the effects of continued size reductions, determine the effective thermal conductivity, and examine the transient operational characteristics and performance limitations of these devices.

Received 7 January 2000; presented as Paper 2000-0969 at the 38th Aerospace Sciences Meeting, Reno, NV, 10–13 January 2000; revision received 17 April 2000; accepted for publication 19 April 2000.

*Graduate Research Assistant, Department of Mechanical Engineering; y0w6809@acs.tamu.edu. Student Member AIAA.

†Assistant Professor, Department of Mechanical and Aerospace Engineering.

‡Provost, Troy Building, Room 3018; peterson@rpi.edu.

Table 1 Configuration of micro heat pipe

Prototype	Material	Working fluid	Total dimension, mm	Thickness of sheet, mm	Diameter of wire, mm	Number of wires	Evaporator size, mm
1	Aluminum	Acetone	152 × 152.4	0.40	0.50	43	25.4 × 152.4
2	Aluminum	Acetone	152 × 152.4	0.40	0.80	43	25.4 × 152.4
3	Aluminum	Acetone	152 × 152.4	0.40	0.50	95	25.4 × 152.4

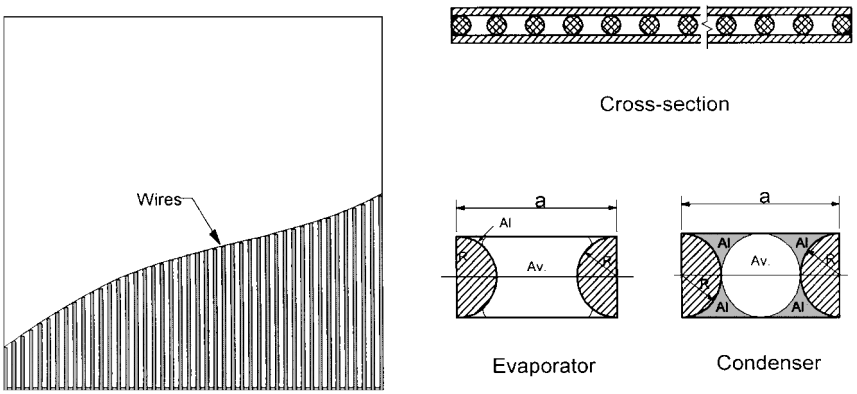

Fig. 1 Micro-heat-pipe array with wires.

These studies have included a combined steady-state analytical and experimental investigation of heat pipes approximately 1 mm^2 in cross-sectional area,[3] a transient investigation of micro heat pipes specifically designed for use in the cooling of ceramic chip carriers,[4] an evaluation of an array of individual micro heat pipes, each approximately 100 μ in diameter either machined or etched into silicon wafers,[5–7] and a study of the limiting factors in determining the maximum heat transport in micro heat pipes.[8–12]

Although almost all of these investigations have provided insight and a better understanding of the heat transport mechanisms occurring in the micro heat pipes, the vast majority of these investigations have focused on a determination of the heat-transport limits. In addition, all of these have used conduction and/or convection heat rejection environments and applications where there are three distinct sections, that is, evaporator, adiabatic section, and condenser. In the current investigation the micro-heat-pipe array is exposed to radiation, and both the evaporator and the condenser emit energy to the environment; no adiabatic section exists. For these reasons the previously developed models cannot be directly employed to predict the temperature distribution of the current design.[13]

To determine the feasibility of using arrays of micro heat pipes, a number of conceptual designs have been developed and evaluated to improve the effective thermal conductivity in the fin structure. The first step in this process was the development of a theoretical model that could be used to predict the temperature distribution of the micro-heat-pipe array. To verify the modeling results, an experimental test facility was developed. Comparison of the theoretical and experimental results provides a variety of information that can be used to design, optimize, and manufacture a flexible, lightweight radiator fin.

Micro-Heat-Pipe Arrays

Based on the requirements outlined in the initial study performed by NASA and Lockheed Martin Vought Systems for the design and development of a highly flexible, reliable, and freeze-resistant radiator, the flexible micro-heat-pipe radiator, illustrated in Fig. 1, was developed. This radiator utilized an array of aluminum wires sintered or brazed between two thin aluminum sheets. The sharp corners formed between the wire and the case material were used as liquid arteries to "pump" the working fluid from the condenser to the evaporator section. In addition to providing capillary pumping, the solid wires were also useful in assisting in freeze prevention and recovery because of their ability to conduct heat axially and directly apply it to the liquid vapor interface. In this design the vapor flows through the microchannels formed between the individual wires.

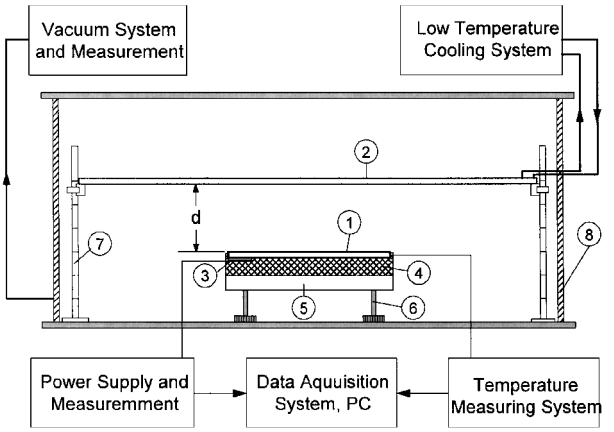

Fig. 2 Experimental system: 1, micro-heat-pipe array; 2, cold plate; 3, electric heater; 4, insulation material; 5, Teflon plate; 6, adjustable support feet; 7, supporter with scaling; and 8, vacuum chamber.

Table 1 lists the physical specifications of the three micro-heat-pipe arrays fabricated. To improve the emissivity and overall reliability, the radiator surfaces were coated with a layer of Flexible Z-93 flat paint. Acetone was used as the working fluid for all tests.

To determine the heat transport capacity and temperature distribution for the micro-heat-pipe arrays investigated, the experimental system, shown in Fig. 2, was developed. This system consisted of a vacuum chamber (235 mm high × 660 mm in diameter), a vacuum pump, a low-temperature system (liquid nitrogen and cooling bath), a copper cold plate (457.2 × 457.2 mm), a power supply and measuring unit, and a data acquisition system (3497A) controlled by a personal computer. The cold plate was painted with black paint in order to improve the emissivity of the surface. The closed chamber and vacuum pump were used to maintain a low-vacuum condition to reduce the effects of convective heat transfer losses. Liquid (or vapor) nitrogen or low-temperature coolant flowing through a cold plate was used to provide the low-temperature environment. Using the liquid nitrogen, the temperature on the surface of the cold plate could be maintained at lower limit of approximately 150 K. A series of thin-film electric heaters were attached to the evaporator section of the micro-heat-pipe array using a high-conductivity silicon adhesive,

as shown in Fig. 2, and the power added to the heater was measured and recorded by the data acquisition system. Twenty-four T-type thermocouples were placed on the micro-heat-pipe array to measure the temperature distribution. In addition, a number of thermocouples were used to monitor the temperature variation on the cold plates and chamber walls. The uncertainty of the measured temperature was less than 0.5°C in the temperature range evaluated.

Prior to the start of the experiment, energy loss tests for the heat added to the evaporator were carried out in order to determine the energy lost as a function of the total energy added to the micro heat pipe. The heat loss was estimated by measuring the temperature difference through the insulation material. For all cases the total heat loss was less that 8.4% of the total power input to the evaporator. Throughout the entire test program the pressure within the test chamber was maintained at less than 10^{-1} torr, effectively eliminating the convective heat losses. Following these baseline tests, the system was allowed to equilibrate for about 30–60 min to reach steady-state conditions, that is, the temperature on the cold plates and vacuum chamber was allowed to reach a constant value. Once the system reached steady-state conditions, the input power and the temperatures on the micro-heat-pipe array, cold plate, and vacuum chamber were recorded.

Numerical Modeling

As illustrated in Fig. 2, the radiator test article with embedded micro-heat-pipe array was placed in the vacuum chamber parallel to the much larger cold plate to simulate the thermal conditions that would be experienced in space. Heat added to the evaporator was uniformly distributed over the evaporator area, that is, a constant heat-flux boundary condition at the evaporator. Because the entire radiator was exposed to a radiation environment, as shown in Fig. 2, the upper surface of the micro-heat-pipe array, including the evaporator and condenser areas, emitted energy to the environment, and as a result no adiabatic section existed. Clearly, for the micro-heat-pipe array working in the radiation environment investigated here, the traditional definitions for the evaporator, adiabatic section, and condenser would not be valid. Likewise, because of the importance of radiation heat transfer, the previously developed model could not be directly employed to predict the heat-transport capability or the temperature distribution.[13]

To simplify the model and provide an approach that could be used to direct the design of flexible spacecraft radiators, the method of effective thermal conductivity was employed. The preliminary experimental data indicated that the temperature difference across the cross section of the micro-heat-pipe array was very small compared with the temperature difference from the evaporating area to the condensing area along the axial direction. It is reasonable, therefore, to assume that the heat-transfer process in the micro-heat-pipe array could be represented as two-dimensional plate conduction combined with a radiation boundary condition.

As shown in Fig. 3, taking a control volume and performing an energy balance the governing equation can be expressed as

$$\frac{\partial}{\partial x}\left(K_{\text{eff},x}\frac{\partial T}{\partial x}\right)+\frac{\partial}{\partial y}\left(K_{\text{eff},y}\frac{\partial T}{\partial y}\right)-q_k+q_0=0 \qquad (1)$$

where $K_{\text{eff},x}=t\cdot k_{\text{eff},x}$ and $K_{\text{eff},y}=t\cdot k_{\text{eff},y}$, in which q_0 is the heat flux added to the control volume k of the evaporation section of the micro-heat-pipe array and q_k is the net radiation transfer through the control volume k, defined as

$$q_k=\frac{\varepsilon_k\left(\sigma T_k^4-J_k\right)}{1-\varepsilon_k} \qquad (2)$$

where J_k is the radiosity.

The more general equation for determining net radiation transfer of surfaces in enclosures when temperature distributions are specified can be expressed as

$$\sum_{j=1}^{n+2}\left(\frac{\delta_{kj}}{\varepsilon_j}-F_{k-j}\frac{1-\varepsilon_j}{\varepsilon_j}\right)q_j=\sum_{j=1}^{n+2}(\delta_{kj}-F_{k-j})\sigma T_j^4 \qquad (3)$$

where δ_{kj} is the Kronecker delta defined as

$$\delta_{kj}=\begin{cases}1 & \text{when} \quad k=j\\ 0 & \text{when} \quad k\neq j\end{cases}$$

Equation (3) can also be used to determine the surface temperatures when the net heat flux is given. In using Eq. (3) to calculate the net heat flux on surfaces in the enclosures, it is assumed that the cold plate acts as the surface $n+1$, and the surface of the closed chamber shown in Fig. 3 is the surface $n+2$. Each surface (i.e., each surface of the control volume on the micro-heat-pipe array, cold surface, and the environment) of the enclosure is assumed to be isothermal and characterized by a uniform radiosity and irradiation. Opaque, diffuse, and gray surface behavior is also assumed.[14]

To solve Eq. (1), it is necessary to determine the appropriate boundary conditions. Because the thickness of the three micro-heat-pipe arrays investigated was on the order of 1–2 mm, the radiation heat transfer at the edges would be very small and was neglected. In this way adiabatic boundary conditions on the edges could be assumed, that is,

$$\frac{\partial T}{\partial x}=0 \qquad \begin{cases}\text{at } x=0, & 0\le y\le 152.4 \text{ mm}\\ \text{at } x=152 \text{ mm}, & 0\le y\le 152.4 \text{ mm}\end{cases}$$

$$\frac{\partial T}{\partial y}=0 \qquad \begin{cases}\text{at } y=0, & 0\le x\le 152 \text{ mm}\\ \text{at } y=152.4 \text{ mm}, & 0\le x\le 152 \text{ mm}\end{cases}$$

$$q_0=q_{\text{input}}, \qquad x\le 25.4 \text{ mm}, \qquad 0\le y\le 152.4 \text{ mm}$$

$$q_0=0, \qquad x>25.4 \text{ mm}, \qquad 0\le y\le 152.4 \text{ mm}$$

To solve Eq. (1) coupled with Eqs. (2) and (3), the view factors and effective thermal conductivities must be known. Because the energy received by a control volume depends on the relative location with respect to the cold surface, that is, the view factor, both integral and Monte Carlo methods were employed.

The effective thermal conductivity of the array along the axial direction was expected to be much larger than the effective thermal conductivity across the array because of the coupling of the micro heat pipes in the axial direction. For a given direction, however, the effective thermal conductivity can be assumed constant and can be measured directly from the experimental results described.

Considering the constant thermal effective conductivity for the micro-heat-pipe array, Eq. (1) can be converted to the discretized equation

$$a_1T_{i-1,j}^n-a_2T_{i,j}^n+a_1T_{i+1,j}^n=c_1-c_2\left(T_{i,j+1}^{n-1}+T_{i,j-1}^{n-1}\right) \qquad (4)$$

where

$$a_1=\frac{K_{\text{eff},x}}{\Delta x^2} \qquad (5)$$

$$a_2=2\left(\frac{K_{\text{eff},x}}{\Delta x^2}+\frac{K_{\text{eff},y}}{\Delta y^2}\right) \qquad (6)$$

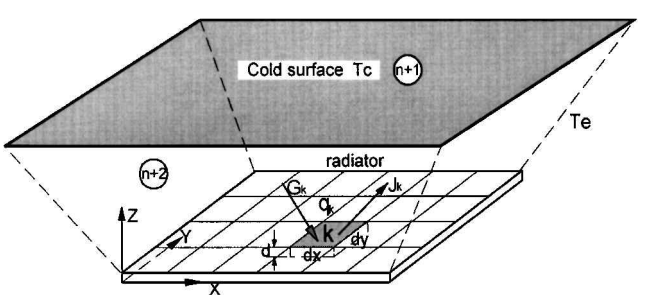

Fig. 3 Schematic of radiation of finite element surfaces in enclosures.

$$c_1 = (q_k - q_0) \tag{7}$$

$$c_2 = \frac{K_{\text{eff},y}}{\Delta y^2} \tag{8}$$

The numerical procedure used for this combined conduction/radiation problem was to first calculate the temperature profile using the conduction equation Eq. (4) with an initial radiation value. The algebraic average temperature was then determined using an iterative averaging algorithm method in order to ensure compliance with the energy balance on the radiator fin. Adding the temperature profile and algebraic average temperature resulted in a new temperature distribution. Once this was known, the radiation distribution was determined using Eq. (3) and a new temperature distribution was determined. This process was repeated using each successive new radiation distribution until the solution converged. Combining the radiation equation, Eq. (3), with the finite difference equation Eq. (4), a solution was achieved using a direction implicit (DI) method in MATLAB®. For steady-state operation the temperature convergence between two successive iterations was less than 10^{-7}, and the energy convergence was also less than 10^{-7}.

Results and Discussion

As already indicated, the effective thermal conductivity is a key factor in determining the temperature distribution occurring in the micro-heat-pipe array using the model developed here. From Fourier's conduction law the effective thermal conductivity of the micro-heat-pipe array was determined by

$$k_{\text{eff}} = \frac{Q_{\text{input}}}{\Delta T_{\max} L_{ch}} \tag{9}$$

where Q_{input} is the measured input power, $\Delta T_{\max}$ is the measured maximum temperature difference between the evaporator and the condenser sections, and L_{ch} is the characteristic parameter, defined as

$$L_{ch} = A_{c,s}/L_{\text{eff}} \tag{10}$$

If the heat pipe array consists of three sections, i.e., evaporator, adiabatic section, and condenser with lengths L_e, L_a, and L_{ch}, respectively, the effective length L_{eff} can be expressed as

$$L_{\text{eff}} = \frac{\int_0^{L_e} \dot{m}\, \mathrm{d}z}{\dot{m}_a} + L_a + \frac{\int_{L_e+L_a}^{L} m\, \mathrm{d}z}{m_a} \tag{11}$$

For uniform heat-flux distribution on the evaporator and condenser, Eq. (11) can be simplified as

$$L_{\text{eff}} = \tfrac{1}{2}L_e + L_a + \tfrac{1}{2}L_c \tag{12}$$

Examining the heat-transfer mechanisms along the y direction (Fig. 1) indicated that the energy was transferred primarily through the thermal conduction because the temperature difference between the two wires was very small and the free convection caused by this temperature difference could be neglected. Combining the thermal conductivities for the quiescent vapor and the aluminum sheets, the effective thermal conductivity along the y direction for the prototypes listed in Table 1 were determined to be 118.2, 96.0, and 118.2 W/mK, respectively, for all of these cases. Here the assumption was made that only the sheets conduct heat through the y direction. The effective thermal conductivity along the axial direction, that is, the x direction, was determined by measuring the maximum temperature difference along the axial direction of the micro-heat-pipe array and the maximum heat transport of the array. The heat input and the maximum temperature difference can be obtained experimentally by adjusting the heat flux and then adjusting the temperature of the coolant to maintain a constant operating temperature as measured by thermocouples attached to the outer surface. The thermal conductivity for the solid aluminum investigated here depends on the components of aluminum alloy and the thermal conductivity; however, this later effect can be neglected. The effective thermal conductivity for the micro-heat-pipe array, however, is largely dependent upon the operating temperature.[3] This is particularly true when the operating temperature is outside the normal range for the working fluid. This procedure was followed until dryout occurred.

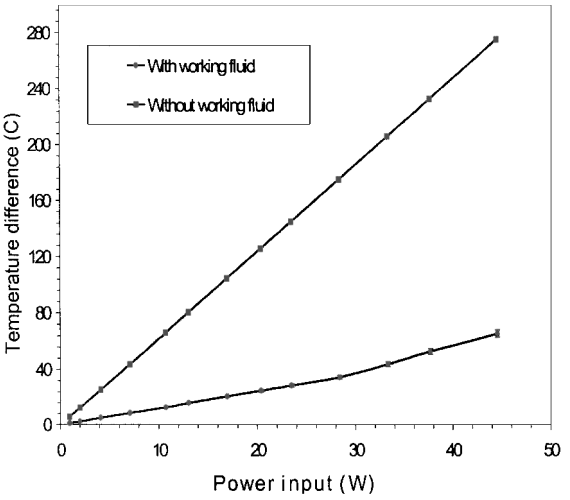

Fig. 4 Temperature difference of micro-heat-pipe arrays with and without working fluid.

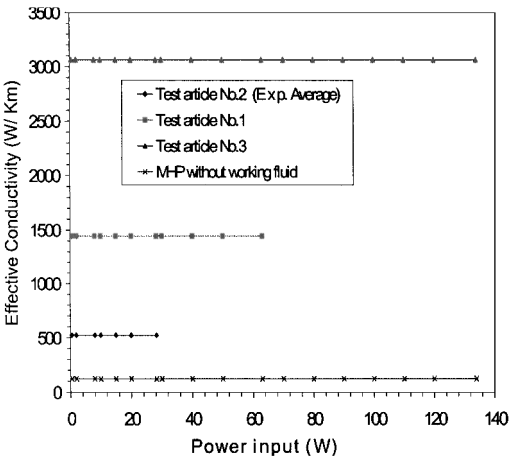

Fig. 5 Effective thermal conductivity of the micro-heat-pipe arrays.

As shown in Fig. 4, the heat transport was nearly proportional to the temperature difference between the evaporator and condenser, i.e., the effective thermal conductivity of the micro-heat-pipe array was nearly constant. Using the measured values for the temperature difference and heat transport, shown in Fig. 4, and the characteristic parameter of the micro-heat-pipe arrays, the effective conductivity could be determined. The resulting values are illustrated in Fig. 5. The effective thermal conductivity for micro-heat-pipe arrays Nos. 1, 2, and 3 were 1446.2, 521.3, and 3023.1 W/Km, respectively. For the micro-heat-pipe arrays without any working fluid, the effective conductivity in the x direction were 126.3, 113.0, and 136.2 W/Km, respectively.

Based on the effective thermal conductivity just obtained and the configurations summarized in Table 1, the temperature distributions for all three micro-heat-pipe arrays were evaluated using the numerical model. All of the numerical calculations shown here used a power input of 19.35 W, and the cold surface and environmental temperatures were 248 and 293 K, for the space and test environments, respectively.

Each of the three cases were modeled both with and without a working fluid charge in order to determine the reduction in the maximum temperature, the mean temperature, and the temperature gradient on the radiator surface. Using the steady-state, two-dimensional conduction equation, coupled with the numerical expression just

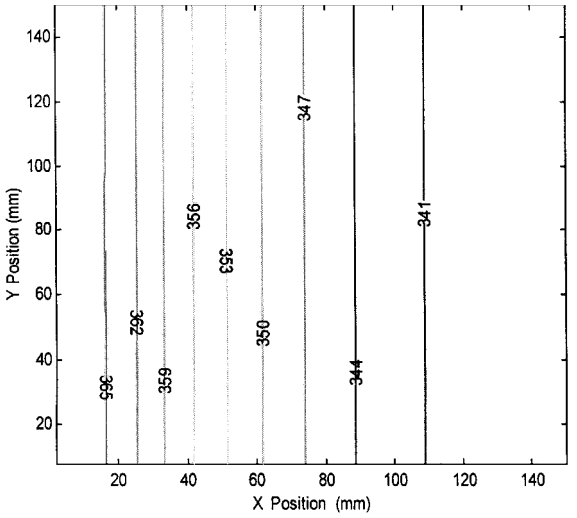

Fig. 6a Temperature distribution predicted by the numerical model for the micro-heat-pipe array without any working fluid in the test environment, P_{input} = 11.8 W.

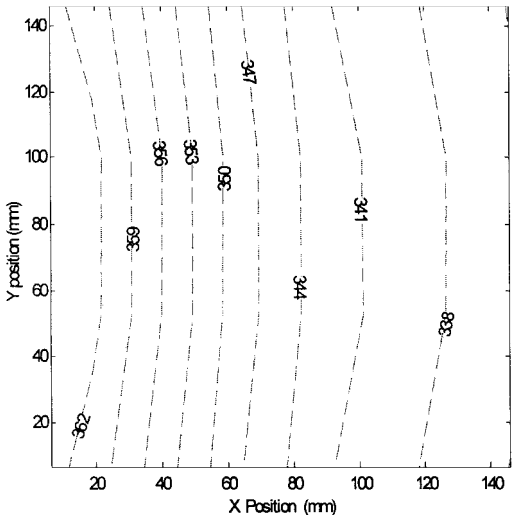

Fig. 6b Temperature distribution obtained experimentally for the micro-heat-pipe array without any working fluid in the test environment, P_{input} = 11.8 W.

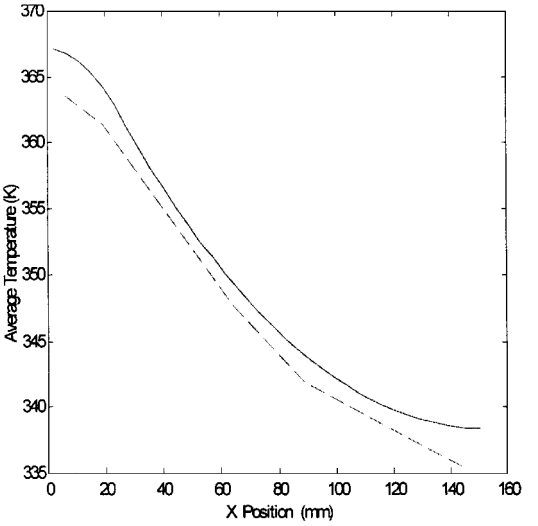

Fig. 7 Comparison of the average temperature along the x direction of the micro heat pipe obtained experimentally and numerically without any working fluid in the test environment, P_{input} = 11.8 W.

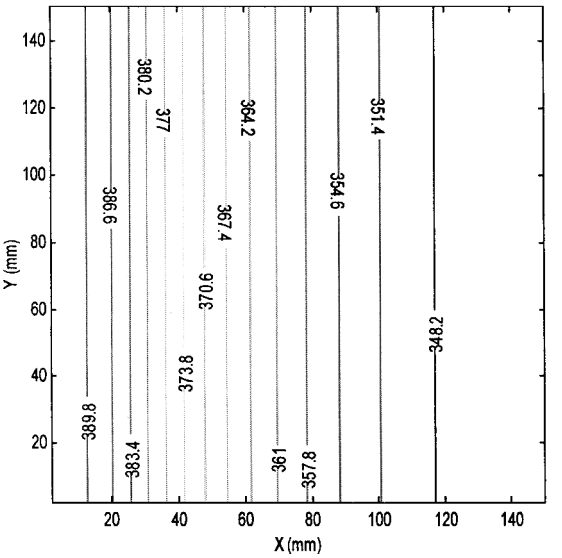

Fig. 8 Temperature distribution for test article no. 1 without any working fluid in a space environment.

developed for radiation, all three micro-heat-pipe radiators were evaluated for a constant source heat flux in both a space environment and a test environment. The space environment was presumed to be an absolute vacuum.

To verify the model developed here, the comparison was first made with the measured experimental data. As shown in Fig. 2, the heat source was provided by an electric film resistance heater with dimensions of 152.4 × 25.4 mm. To verify the modeling approach, the values predicted by the numerical model were compared with experimental results for heat pipe array no. 1 at a power input of 11.8 W. As illustrated in Figs. 6a and 6b, the temperature distribution profiles obtained from the numerical model and experiments were only slightly different. The primary difference was that the experimental results indicated that the isotherms were not uniform in the y direction, that is, the temperature profile was a little higher at the center part than that at the edge. The maximum, minimum, and mean temperatures obtained from the experimental program were 364.2, 334.0, and 347.5 K, respectively. The isotherms predicted by the numerical model were straight lines indicating that the temperature in the y direction was constant and changed only in the x direction; and the maximum, minimum, and mean temperatures were 367.1, 338.4, and 349.3 K, respectively. It is apparent that the temperatures obtained from the experiments were somewhat lower than those obtained from the numerical model for a given point on the radiator surface. To estimate the overall difference between the predicted and measured temperatures, the average temperature along the x direction was determined and is shown in Fig. 7. As indicated, the average temperatures of the numerical calculations were very close to those obtained experimentally, but were consistently lower. The maximum and minimum temperature differences along the x direction obtained by numerical and experimental means were 2.9 and 4.4 K, respectively. The average temperature difference on the surface was 1.8 K. The temperature difference predicted using the numerical model was within 6.8% of the experimental results for all tests conducted. The preceding comparison indicates that the numerical model is valid and can be used to predict the temperature distribution with reasonably good accuracy.

The difference between the two temperature profiles more than likely resulted from radiation heat transfer from the edges of the radiator to the environment (an adiabatic boundary condition was assumed in the numerical model). In addition, there may be some losses caused by conduction introduced by the Teflon supports and the insulation under the heat pipe array and thin film electric heater.

The predicted temperature distribution on the test articles without the working fluids is shown in Figs. 8 and 9 for a power input of

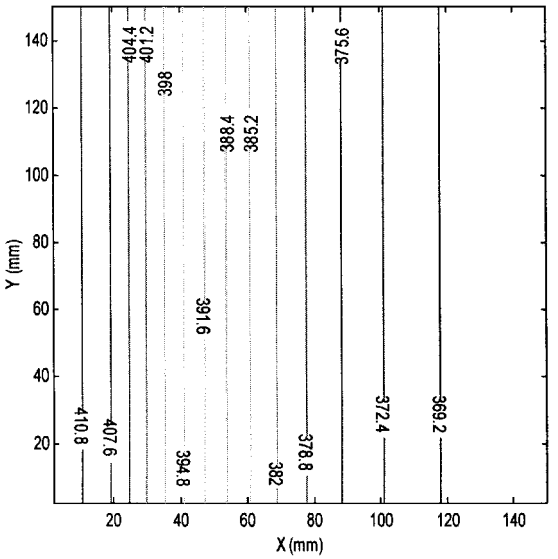

Fig. 9 Temperature distribution for test article no. 1 without any working fluid in the test environment.

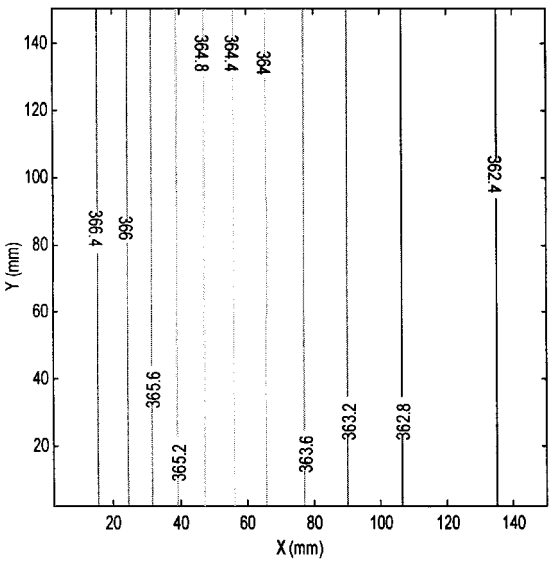

Fig. 10 Temperature distribution for test article no. 1 in a space environment.

19.35 W. The maximum temperature, temperature difference, and average temperature were 391.8, 46.41, and 363.0 K, respectively, in the space environment. In the test environment these values were 412.1, 45.43, and 383.8 K, respectively.

Predicted temperature distributions for test article no. 1 in the two environments are shown in Figs. 10 and 11a. As shown, the maximum temperature, temperature difference, and average temperature were 366.7, 4.34, 362.3 K, respectively, in a space environment, and 387.4, 4.33, and 384.7 K, respectively, in the test environment. The maximum temperature and temperature difference on test article no. 1 were much smaller than those measured for the micro-heat-pipe array without any working fluid for both the space and test environments. In addition, there was a significant reduction in the maximum temperature and temperature gradient. From these results it is clear that the effectiveness of the radiator fin is significantly improved. The same tendency with test articles nos. 2 and 3 are shown in Figs. 11b–11e. Comparing the three cases, micro-heat-pipe no. 3 had the lowest maximum temperature and temperature difference, and no. 2 had the highest.

The temperature gradients in the micro-heat-pipe array were nearly identical; regardless of the environmental conditions, only the maximum temperature and average temperature were different.

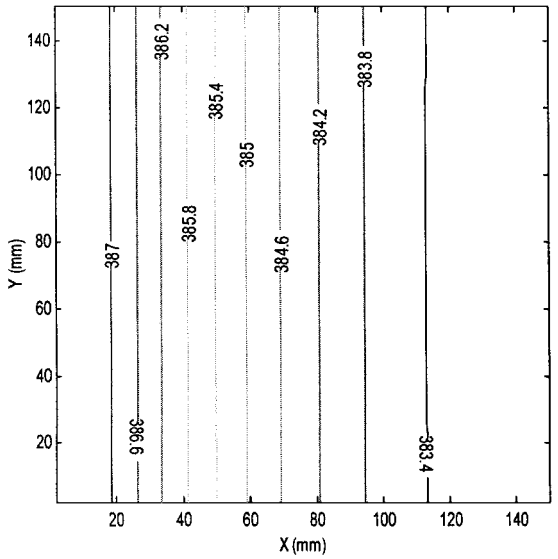

Fig. 11a Temperature distribution for test article no. 1 in a test environment.

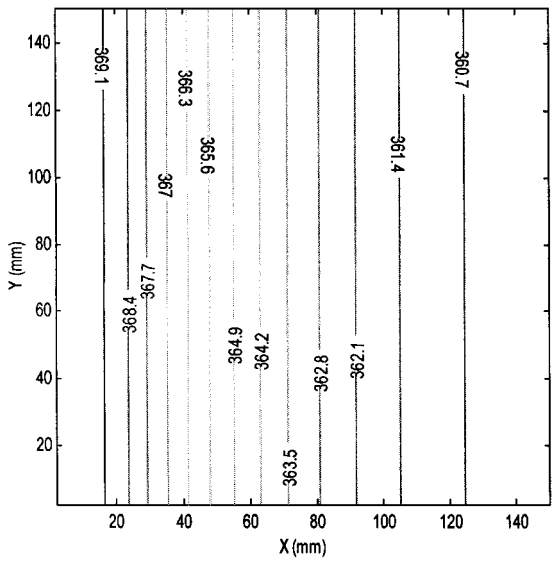

Fig. 11b Temperature distribution for test article no. 2 in the space environment.

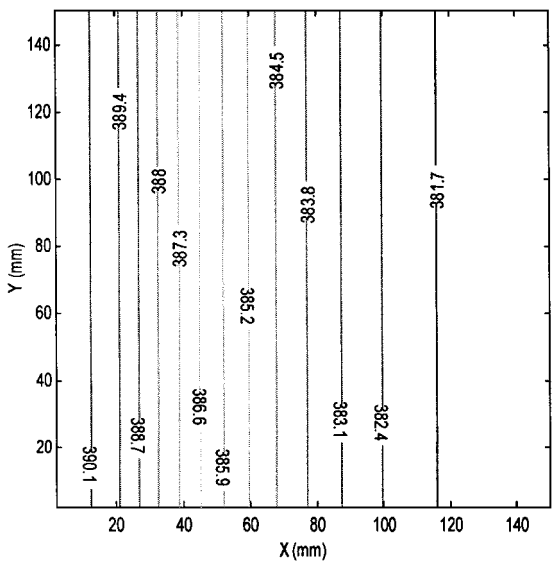

Fig. 11c Temperature distribution for test article no. 2 in the test environment.

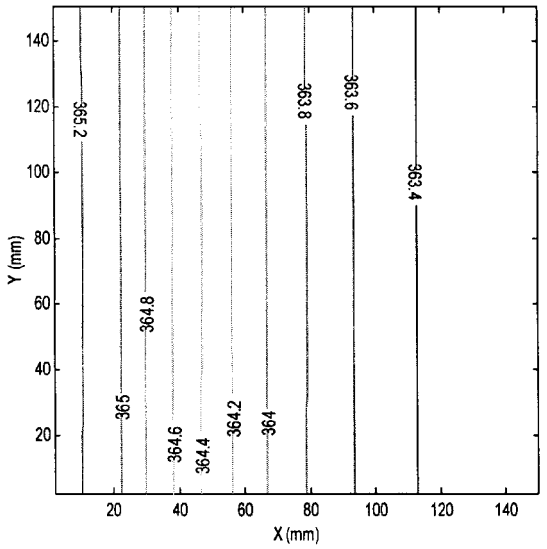

Fig. 11d Temperature distribution for test article no. 3 in the space environment.

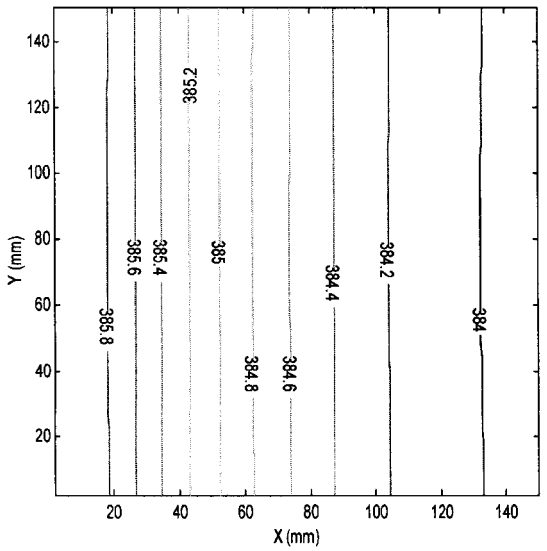

Fig. 11e Temperature distribution for test article no. 3 in the test environment.

This implies that the temperature gradients depend primarily on the characteristics of the heat pipe array and not on the radiation environment. The average temperature decreased with decreases in the environmental temperature because the radiation heat resistance of the radiator increased with the decreasing environmental temperature, that is, a higher average temperature is required to transfer the same amount of heat. For all three heat pipe arrays, both those with and without the working fluid, the average temperatures were nearly the same for the radiation environment and fixed heat source flux. This is consistent with the understanding that the radiation heat transfer depends only on the surface temperature and the environmental temperature for a given surface.

In the design of a phase-change radiator fin for use in a space environment, the heat output and heat source temperature are typically known, making it possible to determine the required heat-transfer area. To determine the heat-transfer rate of the micro-heat-pipe array for a given maximum source temperature, the maximum radiation transport at different evaporating temperatures was investigated.

As illustrated in Fig. 12, the predicted results indicated that heat pipe array no. 3 in a charged condition had the highest overall heat-transport capacity and no. 3 in an uncharged condition had the lowest. For very low operating temperatures, however, all three micro-heat-pipe arrays had nearly identical heat-transport capacities, regardless of their effective thermal conductance. This may have been caused by the radiation resistance of the radiator surface, which was perhaps too large to determine the effect of the somewhat smaller variations in the effective conductivity.

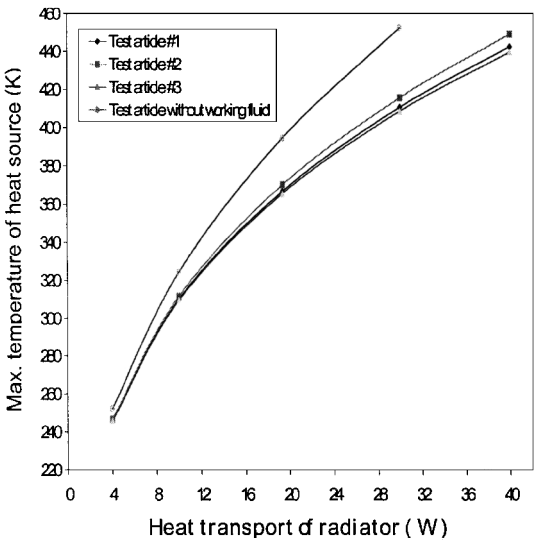

Fig. 12 Comparison of radiation heat transfer of the micro-heat-pipe arrays at different heat source maximum temperatures.

Conclusions

A flexible micro-heat-pipe array, which utilizes an array of metal wires sandwiched between two thin sheets, was developed as a lightweight, flexible radiator fin for use on long-term Mars missions. Three test samples were evaluated, fabricated, and tested. The experimental results indicated that test article no. 3 had the best thermal performance of those tested with a maximum temperature gradient of 2.01 K vs a temperature gradient of 46.4 K for the same test article in an uncharged condition. These results clearly indicated that the presence of the working fluid significantly increased the temperature uniformity on the surface of the micro-heat-pipe fin presented here, and considerably enhances the overall heat-transfer performance.

A numerical model, which combined the effects of conduction and radiation, was established to predict the heat-transfer performance and temperature distribution of the micro-heat-pipe radiator when placed in a space environment. Solution of the resulting finite difference model was accomplished using a DI method. Comparison with the experimental results indicated that the temperature difference predicted by the numerical model was within 6.80% of the experimentally measured values. These results validate the numerical model developed here and indicated that it can be used with confidence to predict the temperature distribution and heat-transfer performance occurring in the flexible micro-heat-pipe radiator described. The small variations between the predicted and measured values may be a result of radiation from the edge of the radiator. The results also indicated that for the size and power levels used in this investigation the micro-heat-pipe radiator did not reach the maximum capillary heat-transport limit.

Acknowledgments

The authors would like to acknowledge the support of the Texas Space Consortium and Lockheed Martin Missiles and Fire Control and in particular Roy Cox for his comments and assistance.

References

[1]Peterson, G. P., *An Introduction to Heat Pipes: Modeling, Testing, and Applications*, Wiley, New York, 1994, pp. 285–321.

[2]Peterson, G. P., "Investigation of Miniature Heat Pipes," Final Rept., Contract F33615-85-c-2733, Task 9, Wright–Patterson AFB, OH, Feb. 1998.

[3]Babin, B. R., Peterson, G. P., and Wu, D., "Steady-State Modeling and Testing of a Micro Heat-Pipe," *Journal of Heat Transfer*, Vol. 112, No. 3, 1990, pp. 595–601.

[4]Wu, D., and Peterson, G. P., "Investigation of Transient Characteristics of Micro Heat Pipes," *Journal of Thermophysics and Heat Transfer*, Vol. 5, No. 1, 1991, pp. 129–134.

[5]Mallik, A. K., and Peterson, G. P., "On the Use of Micro Heat Pipe as an Integral Part of Semiconductor Devices Arrays," *Journal of Electronic Packaging*, Vol. 114, No. 4, 1992, pp. 436–442.

[6]Mallik, A. K., and Peterson, G. P., "Steady-State Investigation of Vapor Deposited Micro Heat Pipe Arrays," *Journal of Electronic Packaging*, Vol. 117, No. 1, 1995, pp. 75–87.

[7]Peterson, G. P., and Mallik, A. K., "Transient Response Characteristics of Vapor Deposited Micro Heat Pipe Arrays," *Journal of Electronic Packaging*, Vol. 117, No. 1, 1995, pp. 82–87.

[8]Ma, H. B., Peterson, G. P., and Lu, X. J., "The Influence of Vapor-Liquid Interactions on the Liquid Pressure Drop in Triangular Microgrooves," *International Journal of Heat and Mass Transfer*, Vol. 37, No. 15, 1994, pp. 2211–2219.

[9]Longtin, J. P., Badran, B., and Gerner, F. M., "A One-Dimensional Model of Micro Heat Pipe During Steady-State Operation," *Journal of Heat Transfer*, Vol. 116, No. 3, 1994, pp. 709–715.

[10]Khrustalev, D., and Faghri, A., "Thermal Analysis of Micro Heat Pipe," *Journal of Heat Transfer*, Vol. 116, No. 3, 1994, pp. 189–198.

[11]Peterson, G. P., and Ma, H. B., "Theoretical Analysis of the Maximum Heat Transport in Triangular Grooves: A Study of Idealized Micro Heat Pipe," *Journal of Heat Transfer*, Vol. 118, No. 3, 1996, pp. 731–739.

[12]Ma, H. B., and Peterson, G. P., "Experimental Investigation of Thermal Capillary Limit of a Novel Micro Heat Pipe Design," AIAA Paper 97-0979, Jan. 1997.

[13]Peterson, G. P., and Ma, H. B., "Temperature Response of Heat Transport in a Micro Heat Pipe," *Journal of Heat Transfer*, Vol. 121, No. 2, 1999, pp. 438–445.

[14]Siegel, R., and Howell, J. R., *Thermal Radiation Heat Transfer*, Taylor and Francis, Washington, DC, 1992, pp. 253–286.